Graphene-based qubits in quantum communications

G. Y. Wu[1,2,*] and N.-Y. Lue[1]

[1]*Department of Physics, National Tsing-Hua University, Hsin-Chu 30013, Taiwan, Republic of China*

[2]*Department of Electrical Engineering, National Tsing-Hua University, Hsin-Chu 30013, Taiwan, Republic of China*

(Received 3 May 2012; published 30 July 2012)

We explore the potential application of graphene-based qubits in photonic quantum communications. In particular, the valley pair qubit in double quantum dots of gapped graphene is investigated as a quantum memory in the implementation of quantum repeaters. For the application envisioned here, our work extends the recent study of the qubit [Wu *et al.*, arXiv:1104.0443; Phys. Rev. B **84**, 195463 (2011)] to the case where the qubit is placed in an in-plane magnetic field configuration. It develops, for the configuration, a method of qubit manipulation, based on a unique ac electric field-induced, valley-orbit interaction-derived mechanism in gapped graphene. It also studies the optical response of graphene quantum dots in the configuration, in terms of valley excitation with respect to photonic polarization, and illustrates faithful photon ↔ valley quantum state transfers. This work suggests the interesting prospect of an all-graphene approach for the solid state components of a quantum network, e.g., quantum computers and quantum memories in communications.

DOI: 10.1103/PhysRevB.86.045456 PACS number(s): 73.63.Kv, 71.70.Ej, 68.65.Pq, 76.20.+q

I. INTRODUCTION

Quantum bits (qubits) are the fundamental units of quantum information exchanged in quantum communications (QCs)[1,2] or processed in quantum computing.[3] Apart from the flying photon qubit, which plays an essential role in QCs, of particular interest among the qubits proposed are the static, solid state ones that utilize the spin[4] or valley[5] degrees of freedom of electrons. Such qubits can be used for storage of quantum information and, moreover, having the structure of gated devices, may be scalable and electrically manipulated, similar to semiconductor IC transistors.

The present work focuses on the potential application of valley-based qubits in QCs, which is based on the unique physical properties of graphene recently discovered[6] and extensively studied.[7] As is well known, graphene is a two-dimensional material of hexagonal lattice, with a distinctive band structure characteristic of a Dirac particle. More importantly, there are two independent energy valleys located, respectively, at K and K′ of the Brillouin zone. A low-lying charge carrier may sit in either of the valleys and is endowed with a binary-valued degree of freedom (d.o.f.) analogous to spin.

It has been conjectured for some time that this valley d.o.f. is suited to the coding of quantum information,[8] and the conjecture is recently realized in the proposal of Ref. 5 by Wu *et al.* It is shown that a valley-based qubit (called valley pair qubit) can be implemented by utilizing two coupled quantum dots (QDs) in gapped graphene [epitaxially grown on SiC (see Ref. 9) or BN (see Ref. 10), for example]. As explained in Ref. 5, a valley pair qubit is basically a two-electron system in the double quantum dots (DQD), with the state space consisting of "valley singlet/triplet states" representing, respectively, logical 0/1 values. Reference 5 develops, for the valley pair qubit, a method of quantum state manipulation suited to the implementation of valley-based quantum computing. It employs a static tilted magnetic field configuration, where the in-plane field freezes the electron spin while the normal field induces an asymmetry between K and K′ valleys, creating a corresponding "valley Zeeman splitting."[11,12] A key element of the method is that the splitting in each QD of the qubit can be tuned independently (with a gate voltage) to create across the qubit DQD a differentiation in the size of splitting, which drives a state transformation for the qubit manipulation. The physics underlying the electric tuning of valley splitting involves a unique, relativistic-type physical mechanism in gapped graphene, namely, the following valley-orbit interaction (VOI) ($\tau_v = +1/-1$ for K / K′, 2Δ = band gap, m^* = electron effective mass, V = potential energy, $\boldsymbol{p}$ = momentum operator):

$$H_{\mathrm{VOI}} = \tau_v \frac{\hbar}{4m^*\Delta} \nabla V \times \vec{p}.$$

The VOI is an analogue of the Rashba mechanism[13] of spin-orbit interaction (SOI). While the SOI has been demonstrated an effective mechanism for electrical manipulation of spin qubits in semiconductors,[14] the VOI provides an alternative mechanism in the case of graphene where the SOI strength is known to be weak.[7]

The present work belongs to the series of our recent theoretical investigations of valley pair qubits, and extends the scope of potential applications for valley pair qubits from quantum computing to photon-based QCs. In particular, it examines the issue of photon ↔ valley quantum state transfer (QST) critical to the application envisioned here, and discusses the feasibility of valley-based quantum memories in the implementation of quantum repeaters for photonic QCs.

It is well known that, with the racing speed of light, photonic QCs hold great promise for quantum networks or long distance distributions of quantum keys in quantum cryptography.[15] In these applications, it is essential to generate with photonic signals a long-range quantum entanglement between two sites. However, due to the exponential decay of photonic signals in the channel, the entanglement usually attenuates with distance, making the long-range distribution of entanglement a challenging task. The quantum repeater protocol is a strategy that solves the problem of attenuation by dividing the channel into many segments and distributing the entanglement in a cascading fashion.[2,16] With the protocol, quantum entanglement is generated in each segment and then

connected with that in the adjacent segment (by entanglement swapping[17]). The same process is applied over and again, each time with the entanglement range being doubled, until eventually it is expanded far enough to cover the two parties (sender and receiver) in the communication. In the protocol, photons are utilized to carry quantum entanglement (over a distance less than the light attenuation length), and solid state qubits are utilized as quantum memories to temporarily store the entanglements already established in the segments. Since the entanglements are built in a probabilistic manner, their storage in solid state qubits is of vital importance in that it synchronizes the entanglements for swapping.

One of the advantages in using solid state quantum memories, such as a semiconductor[18]- or the graphene-based one envisioned here, lies in the accessibility of quantum state manipulation via electrical gate control in the above cascading process. However, important issues arise. For example, an elementary and frequent operation in quantum repeaters with graphene-based quantum memories would be the conversion of a quantum state, from a photonic form to a valley-based one in graphene and vice versa, and it is crucial to minimize the quantum distortion resulting from such quantum state transfers (QSTs). This places a constraint on the working configuration of valley-based qubits, as well as on the corresponding method of state manipulation. The work presented below addresses these important issues.

In the work, we focus primarily on photonic QCs using the photonic polarization ($\sigma+/\sigma-$) for coding. The constraint imposed by a faithful QST then requires that the optical response of graphene QDs be symmetric, in terms of valley excitation with respect to the photonic polarization. In order to see how the constraint arises, consider the following simple example where the valley-based qubit comprises only a single QD-confined electron, with the quantum information being encoded in the linear combination of $|\mathrm{K}\rangle$ and $|\mathrm{K}'\rangle$ (of the electron state). Although the feasibility of quantum information processing based on such a simple qubit has not yet been demonstrated, it provides nonetheless a simple illustration. In this case, a faithful QST from photon to valley qubits means

$$\alpha|\sigma+\rangle + \beta|\sigma-\rangle \rightarrow \alpha|\mathrm{K}\rangle + \beta|\mathrm{K}'\rangle,$$

which can occur, if the QD reacts to an incoming photon symmetrically as follows:

$$\begin{aligned} &|\mathrm{K}(\text{valence})\rangle + |\sigma+\rangle \rightarrow |\mathrm{K}(\text{conduction})\rangle \\ &\qquad\qquad\qquad\qquad (\text{with amplitude M}), \\ &|\mathrm{K}'(\text{valence})\rangle + ||\sigma-\rangle \rightarrow |\mathrm{K}'(\text{conduction})\rangle \\ &\qquad\qquad\qquad\qquad (\text{with amplitude M}'), \\ &|\mathrm{M}| = |\mathrm{M}'|. \end{aligned} \tag{1}$$

In fact, in the absence of a normal magnetic field, the optical excitation in gapped graphene is indeed symmetric, and obeys the selection rule in Eq. (1) approximately, as pointed out previously. [19] With Eq. (1), it follows that

$$\alpha|\sigma+\rangle + \beta|\sigma-\rangle \rightarrow \alpha e^{i\chi}|\mathrm{K}(\text{conduction})\rangle + \beta|\mathrm{K}'(\text{conduction})\rangle \quad (e^{i\chi} = \mathrm{M}/\mathrm{M}'),$$

which is obtained by superposing the two quantum processes in Eq. (1). A further valley state manipulation can be applied to annihilate the extra phase χ appearing in the state, thus achieving a faithful QST from photon to valley qubits. The criterion of a symmetric optical response demonstrated above applies as well to the valley pair qubit considered in the work, as shall soon become clear when we discuss the QST between photon and valley pair qubits.

While the tilted magnetic field configuration works perfectly for quantum computing,[5] the presence of the normal magnetic field component breaks valley symmetry and forbids a symmetric optical response. A focus of the present work is to investigate valley pair qubits in the alternative, in-plane magnetic field configuration, and develop a corresponding method of qubit manipulation in the case.

The presentation is organized as follows. In Sec. II, we provide a description of valley pair qubits in the in-plane magnetic field configuration. In Sec. III, we present the Schrodinger-type equation for electron states in gapped graphene. The equation incorporates relativistic type corrections (RC), including the VOI, up to the second order, and is employed to study an ac electric field-induced VOI-based mechanism. Following the mechanism, the method of state manipulation is developed for valley pair qubits in the in-plane magnetic field configuration. It is shown that the VOI-based mechanism is a second-order relativistic type effect, and an estimate of the effect gives the time scale of $O(10$ ns) for the qubit manipulation. In Sec. IV, we discuss the optical response of graphene QDs, and illustrate the faithful QST from photon to valley pair qubits and vice versa. We also consider the back-to-back QST such as valley $\rightarrow$ photon $\rightarrow$ valley, and show that the QST is highly faithful. In Sec. V, we summarize our findings. In Appendix A, we present the derivation of the Schrodinger-type equation in gapped graphene, with the relativistic-type corrections included up to the second order. In Appendix B, we provide the mathematical details involved in the derivation of the ac electric field-induced VOI-based effect. Finally, in Appendix C, we estimate the coherence time of valley pair qubits in the in-plane magnetic field configuration and show that it can be made long enough for the VOI-based qubit manipulation developed in Sec. III.

II. VALLEY PAIR QUBITS

The pair of coupled QDs (in the x-y plane) for the qubit may be formed by spatially modulating graphene energy bands, e.g., via back gate voltages, to provide a band gap-caused quantum confinement. As shown in Fig. 1(a), electrical gates, V_L, V_R, and V_c, are also placed near the QDs to further modulate the QD confinement potential. In addition, V_c controls the potential barrier between the two QDs and, hence, the corresponding tunneling amplitude $\mathrm{t_{d-d}}$, too. The state of a confined electron is characterized by the following set of indices, (n, X, τ_v, s_x). Here, n is the QD energy level index, $X = \mathrm{L}$ or R, denoting the left / right QD, and $s_x = \pm\frac{1}{2}$ being the electron spin component in the x direction. A static in-plane magnetic field is applied, which freezes the spin degree of freedom at, for example, $s_x = \frac{1}{2}$, as shown in Fig. 1(b).

The Fermi energy is set at such a level that a population of two electrons resides in the DQD structure, interacting

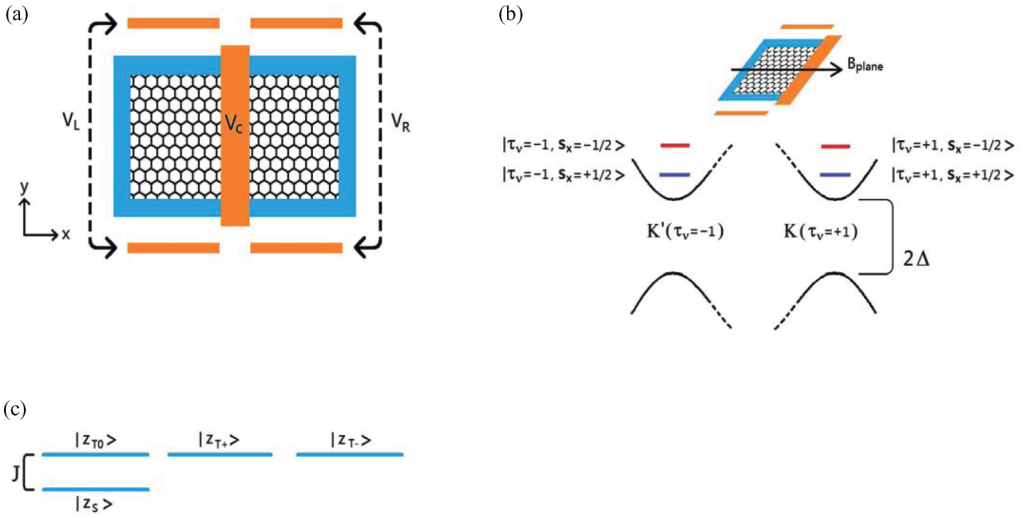

FIG. 1. (Color online) (a) The DQD structure of a valley pair qubit. The QDs are electrostatically defined, for example, by back gates (not shown in the figure). Gate V_c is used to tune the potential barrier and also generate a linear term (in x) in the QD confinement potential. The coupling between the two QDs is characterized by the tunneling amplitude t_{d-d}, and may be controlled by V_c or the back gates. Gates $V_{\rm L}$ and $V_{\rm R}$ are ac biases. (b) A static in-plane magnetic field is applied to freeze the electron spin, leaving only the valley degree of freedom for qubit implementation. (c) Valley singlet (z_S) / triplet (z_{T0}, z_{T+}, z_{T-}) states constitute the low-energy sector of the two-electron states, with the singlet-triplet splitting being given by J.

with each other with the on-site Coulomb repulsion energy (U). The valley pair qubit operates in the low-energy charge configuration ($1_{\rm L}$, $1_{\rm R}$), where the two electrons are separately confined in the QDs with the following exchange-type effective interaction between the electrons:

$$H_J = \tfrac{1}{4} J \vec{\tau}_{\rm L} \cdot \vec{\tau}_{\rm R},$$

with $J \sim 4t_{d-d}^2/(U-\delta\varepsilon)$ being the exchange integral, and $\tau_{\mathbf{L(R)}}$ is the "Pauli valley operator" (identical to Pauli spin operator). $\delta\varepsilon$ here refers to the energy detuning between ($n=0$, $X={\rm L}$, $\tau_{\rm v}$, $s_x=\frac{1}{2}$) and ($n=0$, $X={\rm R}$, $\tau_{\rm v}$, $s_x=\frac{1}{2}$). Note that J is electrically tunable, through the adjustment of t_{d-d} via V_c, or that of $\delta\varepsilon$ via back gate voltages. The eigenstates of H_J are the following valley singlet/triplet states:

$$\begin{aligned}
|z_S\rangle &= \frac{1}{\sqrt{2}}(c^+_{\rm K_L} c^+_{\rm K'_R} - c^+_{\rm K_L'} c^+_{\rm K_R})|{\rm vacuum}\rangle,\\
|z_{T_0}\rangle &= \frac{1}{\sqrt{2}}(c^+_{\rm K_L} c^+_{\rm K'_R} + c^+_{\rm K_L'} c^+_{\rm K_R})|{\rm vacuum}\rangle,\\
|z_{T_+}\rangle &= c^+_{\rm K_L} c^+_{\rm K_R}|{\rm vacuum}\rangle,\\
|z_{T_-}\rangle &= c^+_{\rm K_L'} c^+_{\rm K_R'}|{\rm vacuum}\rangle.
\end{aligned}$$

An exchange splitting (equals J) exists between the singlet $|z_S\rangle$ and the triplet $\{|z_{T_0}\rangle, |z_{T_+}\rangle, |z_{T_-}\rangle\}$, as shown in Fig. 1(c). In the above, ${\rm K_L} = (n=0, {\rm L}, \tau_v = 1)$, and $c^+_{\rm K_L}$ denotes the corresponding electron creation operator. Other notations are similarly defined.

The Hilbert space expanded by $|z_S\rangle$ and $|z_{T_0}\rangle$ constitutes the qubit state space (denoted as $\Gamma_{\boldsymbol{v}}$). $\Gamma_{\boldsymbol{v}}$ is isomorphic to the spin-1/2 state space and, hence, can be represented by the surface of a sphere (i.e., the Bloch sphere). $|z_{T_+}\rangle$ and $|z_{T_-}\rangle$ are outside $\Gamma_{\boldsymbol{v}}$ and not needed in the application of quantum computing/communications. Physically, they are coupled to $|z_S\rangle$ and $|z_{T_0}\rangle$ by the intervalley scattering ${\rm K} \leftrightarrow {\rm K}'$ and provide a channel of leakage contributing to qubit decoherence. In Appendix C, the intervalley scattering of a QD-confined electron is considered.[20]

Valley pair qubits can be manipulated all electrically. For example, if the exchange coupling J is maintained for a duration of t_z, it produces the unitary transformation, $R_z(\theta_z)$, i.e., a rotation about the z axis of the Bloch sphere with the angle of rotation $\theta_z = J\, t_z/\hbar$.[5] However, in order to manipulate the qubit to an arbitrary point on the Bloch sphere, we need, in addition to R_z, a second independent state transformation. Section III addresses this important issue and shows how to produce a rotation about the x axis of the Bloch sphere (called $R_{\rm x}$ below).

Quantum states of valley pair qubits are analogous to spin singlet/triplet states in the spin pair scheme.[21,22] As such, valley pair qubits are characterized by the same distinctive advantages provided in the scheme, e.g., scalability and decoherence-free state space. The method developed in the scheme for initialization/readout/two-bit qugate (CPHASE) operation, as described by Taylor *et al.*,[14] may also be adapted here. With the method and the single qubit operations R_x and R_z, universal quantum computing[23] can be achieved using valley-pair qubits.

III. VOI-BASED STATE MANIPULATION

We note that the valley pair states, $|x_-\rangle$ and $|x_+\rangle$, defined as

$$\begin{aligned}
|x_-\rangle &= \frac{1}{\sqrt{2}}(|z_{T_0}\rangle - |z_S\rangle) = c^+_{\rm K_L'} c^+_{\rm K_R}|{\rm vacuum}\rangle,\\
|x_+\rangle &= \frac{1}{\sqrt{2}}(|z_{T_0}\rangle + |z_S\rangle) = c^+_{K_L} c^+_{\rm K_R'}|{\rm vacuum}\rangle,
\end{aligned}$$

correspond to $|s_x=-1/2\rangle$ and $|s_x=1/2\rangle$, respectively, as implied by the isomorphism between $\boldsymbol{\Gamma}_{\mathbf{v}}$ and the spin-1/2 state

space. Comparing the expressions of $|x_-\rangle$ and $|x_+\rangle$, one sees that if one can break the symmetry between K ($\tau_v = 1$) and K′ ($\tau_v = -1$) in one or both of the QDs, then a differentiation may be created between $|x_-\rangle$ and $|x_+\rangle$ leading to the following contrasting time evolution, namely,

$$|x_-\rangle \rightarrow e^{-i\Phi}|x_-\rangle, \quad |x_+\rangle \rightarrow e^{i\Phi}|x_+\rangle,$$

i.e., a rotation about the x axis of the Bloch sphere.

There are two approaches to produce the needed valley asymmetry. Firstly, a normal magnetic field may be applied, as in the proposal of Wu *et al*. for quantum computing.[5] For QCs, if the same approach is employed, the field would have to be switched on and off frequently (e.g., off during the photon $\leftrightarrow$ valley QST, in order to achieve a faithful QST, and on when the valley qubit is being processed in the quantum repeater) at the same frequency used in sending/receiving the photonic signal, leading to complications in the application. Or, alternatively, one may resort to the second approach where an in-plane magnetic field configuration is employed. In the following, we consider a QD-confined electron in this configuration, and show that an ac electric field can replace the normal magnetic field and induce the required valley asymmetry. This is termed the ac electric field-induced VOI-based effect, and it enables a rotation about the x axis of the Bloch sphere.

A. The QD profile

Apart from the ac electric field, the VOI-based effect depends also on the QD confinement potential. We describe briefly this dependence here. Let $V_{\rm QD}$ be the QD confinement potential. Two profiles are considered. In one case, $V_{\rm QD} = V_2(x,y) + V_3(x)$, with $V_2(x,y) = 1/2\, m^* w_0^2(x^2 + s^2y^2)$ and $V_3(x) = 1/3\, m^* w_0^2 k_{3x} x^3$. "$s$" in V_2 parameterizes the anisotropy of a generic quadratic potential and is taken to be of the order of unity. "k_{3x}" in V_3 characterizes the strength of the cubic potential. In the other case, $V_{\rm QD} = V_2(x,y) + e\,\varepsilon_x\, x + V_4(x)$, involving an electric field (ε_x) in the x direction and a quartic potential $V_4(x) = 1/4 m^* w_0^2\, k_{4x} x^4$. "$k_{4x}$" in V_4 characterizes the strength of the quartic potential, and ε_x may be produced by gate V_c in Fig. 1(a). In either case, in the presence of an ac electric field, the total potential energy of the electron is taken to be $V(x,y) = V_{\rm QD} + V_{\rm ac}$, with $V_{\rm ac} = e\,\varepsilon_y\, \sin(w_s t)\, y$ being the time-dependent potential due to the ac electric field. Here, the corresponding ac electric field, $\varepsilon_y \sin(w_s t)$, is taken in the y direction, and may be produced by gate $V_{\rm L}$ or $V_{\rm R}$ in Fig. 1(a).

As shall become clear below, in the cubic case, the ac electric field-induced VOI-based effect scales with k_{3x} (and thus vanishes in the absence of V_3). Therefore, the presence of V_3 in $V_{\rm QD}$ is an important requirement here. In the quartic case, the electric field ε_x displaces the electron to a new equilibrium position ($x_0 = e\,\varepsilon_x/m^* w_0^2$), and a cubic term appears when $V_{\rm QD}$ is expanded around x_0. This also enables the VOI-based effect.

B. The Schrodinger-type equation with "relativistic correction" up to the second order

Generally, the two-band model (i.e., the Dirac equation) is a good description of both the conduction and valence bands in graphene.[7] However, in order to facilitate an analytical study of the VOI-based effect, we focus here on the regime where the electron is near the conduction band edge, i.e., $E/\Delta \ll 1$, where E is the electron energy with respect to the band edge. (The study can easily be extended to near-band-edge valence band holes.) In this regime, the Dirac equation is reduced to the Schrodinger-type equation derived in Appendix A. In the cubic case where $V_{\rm QD} = V_2(x,y) + V_3(x)$, we have

$$H(x,y,t)\psi(x,y,t) = i\hbar\partial_t\psi(x,y,t), \quad H(x,y,t) = H^{(0)}(x,y,t) + V_3(x) + H^{(1)}(x,y,t) + H^{(2)}(x,y,t),$$
$$H^{(0)}(x,y,t) = \frac{\vec{p}^2}{2m^*} + V_2[x, y + y_0(t)] - \frac{1}{2}m^* w_0^2 y_0^2(t), y_0(t) = \frac{e\varepsilon_y \sin w_s t}{m^* w_0^2}. \tag{2}$$

$y_0(t)$ here is the time-dependent electron displacement due to the ac electric field.

Equation (2) is correct to $O(E/\Delta)^2$. $H^{(0)}$ in the Hamiltonian describes a standard quantum harmonic oscillator (QHO). We consider the weak-field limit where $|y_0| \ll Y$ [$Y = (\hbar/m^* w_0)^{1/2}$ being the size of the QHO oscillation amplitude] and ignore the y_0^2 term in $H^{(0)}$. This linearization does not affect the discussion below, since as will become clear, the leading order of VOI-based effect is linear in y_0. $H^{(0)} + V_3$ constitutes the "nonrelativistic" part of the Hamiltonian. $H^{(1)}$ and $H^{(2)}$ are, respectively, the first- and second-order relativistic-type corrections, with $\|H^{(1)}\|/\|H^{(0)} + V_3\| \sim O(E/\Delta)$ and $\|H^{(2)}\|/\|H^{(0)} + V_3\| \sim O(E^2/\Delta^2)$.

We separate, in $H^{(1)}$ and $H^{(2)}$, valley-dependent and -independent terms. Specifically, we write

$$H^{(1)} = H_0^{(1)} + H_\tau^{(1)}, \quad H_0^{(1)} = -\frac{\vec{p}^4}{8m^{*2}\Delta} - \frac{1}{8m^*\Delta}(\vec{p}^2 V_2) - \frac{1}{8m^*\Delta}(\vec{p}^2 V_3),$$
$$H_\tau^{(1)} = \tau_v \frac{\hbar}{4m^*\Delta}\{\nabla V_2[x, y + y_0(t)]\} \times \vec{p} + \tau_v \frac{\hbar}{4m^*\Delta}(\nabla V_3) \times \vec{p}(\text{first} - \text{orderVOI}). \tag{3}$$

The subscripts "τ"/"0" here label valley-dependent/independent terms. $y_0(t)$ is explicitly written where the time dependence appears. $H^{(1)}$ was previously derived and compared to the first-order relativistic correction (RC) in the standard Schrodinger equation of electrons.[24] For example, the first term in $H_0^{(1)}$ is the RC to the kinetic energy, and the second and the third terms in $H_0^{(1)}$ are the Darwin's term. The second term in $H_0^{(1)}$ is a constant and shall be dropped below, with no effect on the treatment.

$H_\tau^{(1)}$ is the first-order valley-orbit interaction, the analogue of spin-orbit interaction. Similarly, for $H^{(2)}$, we write

$$H^{(2)} = H_0^{(2)} + H_\tau^{(2)}, \quad H_\tau^{(2)} = H_{\tau 2}^{(2)} + H_{\tau 3}^{(2)}(\text{second} - \text{order VOI}),$$
$$H_{\tau 2}^{(2)} = -\tau_v \frac{3\hbar}{32m^{*2}\Delta^2}\{\underline{\nabla V_2[x,y+y_0(t)]\times\vec{p}}\,\vec{p}^2 + \vec{p}^2\underline{\nabla V_2[x,y+y_0(t)]\times\vec{p}}\}, \quad H_{\tau 3}^{(2)} = -\tau_v \frac{3\hbar}{32m^{*2}\Delta^2}[\underline{\nabla V_3\times\vec{p}}\,\vec{p}^2 + \vec{p}^2\underline{\nabla V_3\times\vec{p}}]. \tag{4}$$

$H_\tau^{(2)}$ is the second-order VOI, and has been decomposed into V_2- and V_3- erived terms. Expressions underlined are evaluated first. $H_0^{(2)}$ is not given here, as it is irrelevant to the calculation of the VOI-based effect. See Appendix B. Note that the linearization of $H(x,y,t)$ in y_0 leads to the approximation that $H(x,y,t) \approx H[x,y+y_0(t)]$, as can be verified with Eqs. (2)–(4).

The analysis of VOI-based effect is carried out for the ground state, within the perturbation-theoretical framework where $H^{(0)}$ in Eq. (2) is treated as the dominant term and V_3, $H^{(1)}$, and $H^{(2)}$ are treated perturbatively. The conditions required for the perturbative calculation and the various energy scales involved are summarized below. First of all, $y_0 \ll Y$ and $\|H^{(2)}\| \ll \|H^{(1)}\| \ll \|H^{(0)}\|$, both of which have already appeared or been assumed above. We further take $\|V_3\| \ll \|H^{(0)}\|$ in order for $H^{(0)}$ to be the only dominant term in H. It leads to the following estimate of energy scales, namely, $||H^{(0)}|| \sim E \sim w_0 \ll \Delta, ||H^{(1)}|| \sim O(\hbar^2 w_0^2/\Delta)$, and $||H^{(2)}|| \sim O(\hbar^3 w_0^3/\Delta^2)$. We also assume the adiabatic condition, i.e., $w_s \ll w_0$, meaning that the ac field varies slowly in the time scale of the electron orbital motion. This permits us to employ the adiabatic perturbation theory to treat the time-dependence of *H(t)* due to the ac electric field. We note, in practical applications, that most of the above conditions can actually be relaxed, e.g., $\hbar w_0 \sim \Delta, ||H^{(2)}|| \sim ||H^{(1)}|| \sim ||H^{(0)}||$,or$||V_3|| \sim ||H^{(0)}||$. In such cases, the Dirac equation and/or numerical work are required in an accurate analysis of the VOI-based effect, but the analytic calculation and result presented below can still serve as a useful guidance.

C. Adiabatic perturbation-theoretical treatment

We now perform the quantitative analysis of VOI-based effect. Specifically, we examine if the ac electric field is able to induce any valley dependence in the ground state of the QD-confined electron. We employ the adiabatic perturbation theory[25] and write the ground-state wave function

$$\psi_0(x,y,t) \approx \varphi_0[x,y+y_0(t)]e^{-\frac{i}{\hbar}\int^t E_0(t')dt'} e^{\frac{i}{\hbar}\int^t \gamma_0(t')dt'}. \tag{5}$$

Here, $\varphi_0(t)$ and $E_0(t)$ are the instantaneous ground state and energy, respectively, defined in the following:

$$H[x,y+y_0(t)]\varphi_0[x,y+y_0(t)] = E_0(t)\varphi_0[x,y+y_0(t)]. \tag{6}$$

$\int_t E_0(t')dt'/\hbar$ and $\int_t \gamma_0(t')dt'/\hbar$ in Eq. (5) are, respectively, the dynamical and the geometric phases of the state. Equation (6) has the following useful symmetry properties. Firstly, using the expression of $H(t)$ provided in Eqs. (2)–(4), one can show that $H(\tau_v = -1) = H^*(\tau_v = 1)$. Therefore, if $\varphi_0(t)$ is an eigenstate solution in Eq. (6) for $\tau_v = 1$, then $\varphi_0^*(t)$ is an eigenstate for $\tau_v = -1$, and both states are degenerate with the same energy $E_0(t)$. Accordingly, the ac field does not generate any valley dependence in $E_0(t)$, or in the dynamic phase. This is basically a consequence of the time-reversal symmetry for valley states. Secondly, in the case where $V_3(x)$ is absent, we have $V_{QD}(x,y) = V_{QD}(-x,y)$ and hence $H(x,y) = H^*(-x,y)$. It follows that $\varphi_0(x,y) = \varphi_0^*(-x,y)$ as a result of the reflection symmetry. This fact shall be used later.

Substitution of the wave function (5) into the Schrodinger equation (2) yields γ_0, the rate of change in the geometric phase,

$$\begin{aligned}\gamma_0(t) &= i\hbar\langle\varphi_0[x,y+y_0(t)]|\partial_t\varphi_0[x,y+y_0(t)]\rangle \\ &= -[\partial_t y_0(t)]\langle\varphi_0(x,y)|p_y\varphi_0(x,y)\rangle.\end{aligned} \tag{7}$$

Note, in the second line, that $y_0(t) = 0$ in $\langle\varphi_0(\tau_v)|p_y\varphi_0(\tau_v)\rangle$. Therefore we have the property (i) γ_0 is linear in y_0. Property (i) justifies the linearization of H in y_0, in the analysis of VOI-based effect. Using the time reversal property $\varphi_0(\tau_v = -1) = \varphi_0^*(\tau_v = 1)$ in Eq. (7) yields (ii) $\langle\varphi_0(\tau_v)|p_y\varphi_0(\tau_v)\rangle \propto \tau_v$ or $\gamma_0 \propto \tau_v$. Condition (ii) shows that being valley dependent, γ_0 is able to generate a valley-contrasting time evolution sought in the beginning of the section. Furthermore, in the case where V_3 is absent, the reflection property $\varphi_0(x,y) = \varphi_0^*(-x,y)$ mentioned earlier yields $\gamma_0 = 0$ in Eq. (7). This implies that (iii) $\gamma_0 \propto k_{3x}$. Collecting (i)–(iii), we write

$$\gamma_0(t) \propto \tau_v\,[\partial_t y_0(t)]\,k_{3x}. \tag{8}$$

This result serves as a useful guide in the evaluation of γ_0 below.

D. γ_0 in the cubic case

In Eq. (7), the adiabatic perturbative calculation has isolated the time dependence of γ_0, leaving only the time-independent expectation value, $\langle\varphi_0|p_y\varphi_0\rangle|_{y_0=0}$, to be evaluated, with φ_0 now determined by the following (*time-independent*) equation:

$$\begin{aligned}H|_{y_0=0}\varphi_0(x,y) &= E_0\varphi_0(x,y), \quad H = H^{(0)} + V_3 + H', \\ H' &= H^{(1)} + H^{(2)}.\end{aligned} \tag{9}$$

The notation H' is introduced above, and is to be treated within the time-independent perturbation theory in the evaluation of $\langle\varphi_0|p_y\varphi_0\rangle|_{y_0=0}$. (From now on, the subscript $y_0 = 0$ shall be dropped.)

Utilizing the fact that $\langle\varphi_0(\tau_v)|p_y\varphi_0(\tau_v)\rangle \propto \tau_v$, derived earlier, we write

$$\langle\varphi_0(x,y)|p_y\varphi_0(x,y)\rangle \approx p_y^{(1)} + p_y^{(2,1)} + p_y^{(2,2)}, \tag{10}$$

which is correct to the second-order RC $p_y^{(1)}$ is the first-order RC and derived from $H_\tau^{(1)}$ in the first-order perturbative treatment of H'. $p_y^{(2,1)}$ denotes the first-order RC, derived from $H_\tau^{(1)}$, in the second-order perturbative treatment of H'. $p_y^{(2,2)}$ denotes the second-order RC, derived from $H_\tau^{(2)}$, in the

first-order perturbative treatment of H'. We summarize these perturbative results below:

$$p_y^{(1)} = 0,$$
$$p_y^{(2,1)} = -\tau_v \frac{s}{64}\left[-2 + \frac{4}{s} - \frac{16}{3(s+1)} + \frac{50}{3(s+2)}\right]\hbar\frac{\hbar^2 w_0^2}{\Delta^2}k_{3x},$$
$$p_y^{(2,2)} = \tau_v \frac{1}{16}\hbar\frac{\hbar^2 w_0^2}{\Delta^2}k_{3x}. \quad (11)$$

For details of the derivation, see Appendix B. Overall, this gives

$$\gamma_0(t) = C_3\tau_v\hbar(\partial_t y_0)\frac{\hbar^2 w_0^2}{\Delta^2}k_{3x},$$
$$C_3 = \frac{s}{96}\left[-3 - \frac{8}{s+1} + \frac{25}{s+2}\right]. \quad (12)$$

We stress that because $p_y^{(1)} = 0$, an analysis correct only to the first-order RC here would have yielded a vanishing γ_0. The finite result shown in Eq. (12) is basically a *second-order relativistic type effect* involving the VOI ($H_\tau{}^{(1)}$ and $H_\tau{}^{(2)}$).

E. γ_0 in the quartic case

We extend the result (12) to the quartic case where $V_{\rm QD} = V_2(x,y) + e\,\varepsilon_x\,x + V_4(x)$, with $V_4(x) = 1/4m^* w_0^2 k_{4x}x^4$. For $k_{4x} < 0$, the potential $V_2(x,y) + V_4(x)$ is a realistic description of a finite, symmetric confinement potential in the x direction.

In the limit of weak ε_x (with $x_0 \ll Y$), expansion of $V_{\rm QD}$ around x_0 leads to

$$V_{QD} = V_2(x,y) + e\varepsilon_x x + V_4(x)$$
$$\overset{x'=x+x_0}{\approx} V_2(x',y) + V_4(x',y) - m^* w_0^2 k_{4x}x_0 x'^3.$$

Here, nonlinear terms of x_0 have been dropped. The result shows that the electric field produces effectively a cubic term in the potential with the strength $k_{3x} = -3k_{4x}x_0$. In the limit where $|V_4| \ll V_2$, we substitute the effective k_{3x} into Eq. (12), yielding

$$\gamma_0(t) = C_4(s)\tau_v\hbar(\partial_t y_0)\frac{\hbar^2 w_0^2}{\Delta^2}k_{4x}x_0,$$
$$C_4(s) = -\frac{s}{32}\left[-3 - \frac{8}{s+1} + \frac{25}{s+2}\right]. \quad (13)$$

C_4 can be optimized, by a choice of the parameter s (i.e., the QD shape). We briefly note the following. In the case of an isotropic potential ($s = 1$), $C_4 = -1/24$. In the anisotropic case, C_4 varies slowly with s, with

$$|C_4| > \tfrac{1}{24} \quad \text{for} \quad s < 1 \quad \text{and} \quad |C_4| < \tfrac{1}{24} \quad \text{for} \quad s > 1.$$

In practical applications, the conditions, $x_0 \ll Y$ and $|V_4| \ll V_2$, used in the derivation of Eq. (13), can be relaxed, e.g., $x_0 \sim Y$ and $|V_4| \sim V_2$.

F. Qubit manipulation

For illustration, we consider the qubit manipulation in the quartic case. As made clear in the above, a geometric phase contrast is induced by the ac electric field between valley states. In half of the ac cycle ($-\pi/2w_s$, $\pi/2w_s$), for example, it evolves as follows:

$$|\mathrm{K}\rangle \to |\mathrm{K}\rangle e^{i\Phi_{1/2}}, \quad |\mathrm{K}'\rangle \to |\mathrm{K}'\rangle e^{-i\Phi_{1/2}},$$
$$\Phi_{1/2} = \frac{1}{\hbar}\int_{-\pi/2w_s}^{\pi/2w_s}\gamma_0(t';\tau_v = 1)dt' = \frac{y_0^{(\max)}}{l_{vo}}, \quad (14)$$
$$y_0^{(\max)} = \frac{e\varepsilon_y}{m^* w_0^2}, \quad l_{vo} = \left(2C_4\frac{\hbar^2 w_0^2}{\Delta^2}k_{4x}x_0\right)^{-1}.$$

Here, $y_0^{(\max)}$ is the electron displacement amplitude due to the ac field, and $l_{\rm vo}$ is called the valley-orbit length.

In the case of a valley pair qubit, the foregoing phase contrast results in a qubit state transformation as follows. Let us consider the simple mode of manipulation where the exchange interaction J between the QDs is turned down when both QDs (or just one of them) are subject to ac electric fields. For $J/\hbar \ll w_s$, it freezes the interdot orbital motion, $|\mathrm{K_L\,K'_R}\rangle \leftrightarrow |\mathrm{K'_L K_R}\rangle$, and hence the associated J-induced R_z during the action of the ac fields. Based on Eq. (14), the ac fields produce the following evolution of valley pair states in half of the ac cycle:

$$\begin{matrix}|\mathrm{K_L K'_R}\rangle \to e^{i\theta_x/2}|\mathrm{K_L K'_R}\rangle \\ |\mathrm{K'_L K_R}\rangle \to e^{-i\theta_x/2}|\mathrm{K'_L K_R}\rangle\end{matrix}, \text{ or } \begin{matrix}|x_+\rangle \to e^{i\theta_x/2}|x_+\rangle \\ |x\rangle \to e^{-i\theta_x/2}|x_-\rangle\end{matrix},$$
$$\frac{\theta_x}{2} = \frac{y_{0,L}^{(\max)}}{l_{\mathrm{vo},L}} - \frac{y_{0,R}^{(\max)}}{l_{\mathrm{vo},R}}. \quad (15)$$

Here, $y_{0,\mathrm{L(R)}}^{(\max)}$ is the ac field-induced electron displacement amplitude in $\mathrm{QD_{L(R)}}$, and $l_{\mathrm{vo,L(R)}}$ is the valley-orbit length for $\mathrm{QD_{L(R)}}$. Equation (15) represents a state rotation about the x axis, $R_x(\theta_x)$. Combining $R_x(\theta_x)$ and $R_z(\theta_z)$, one can manipulate the qubit to an arbitrary point on the Bloch sphere (see Fig. 2).

We give below a numerical estimate of the time (denoted as $t_{\rm operation}$) needed for a typical single qubit manipulation. It is assumed that a series of alternate $R_x(\theta_x)$'s and $R_z(\theta_z = \pi)$'s are used in the manipulation, as shown in Fig. 2. We take $\pi/w_s \sim 0.1$ ns. Moreover, J in the range of 1 meV or lower is achievable.[5] Therefore the time ($\pi\hbar/J$) spent on each $R_z(\theta_z = \pi)$ can be made much less than or comparable to the time (π/w_s) on each $R_x(\theta_x)$. Accordingly, $t_{\rm operation}$ is determined primarily by the total time spent on $R_x(\theta_x)$'s, and it leads to the estimate that $t_{\rm operation} \sim O[\pi/w_s\theta_x]$. Using $k_{4x} = L^{-2}$ (L = QD size), $x_0 = 0.3L$, $s = 1$, and $\hbar w_0/\Delta = 0.5$, Eq. (14) gives $l_{\mathrm{vo,L(R)}} \sim 120L$. For $y_{0,\mathrm{L}}^{(\max)} = -y_{0,\mathrm{R}}^{(\max)} = 0.3L$, and $\pi/w_s = 0.1$ ns, Eq. (15) gives $\theta_x = 0.01$ and thus $t_{\rm operation} \sim O(10\ \mathrm{ns})$.

IV. OPTICAL RESPONSE AND QUANTUM STATE TRANSFER

Firstly, we describe the near-band-gap optical response from a gapped graphene QD. In particular, we consider the excitation of an electron from a valence band state to the lowest quantized conduction band state in the QD, as shown in Fig. 3.

Since the excitation involves both valence and conduction bands, we return to the two-band model, i.e., the Dirac

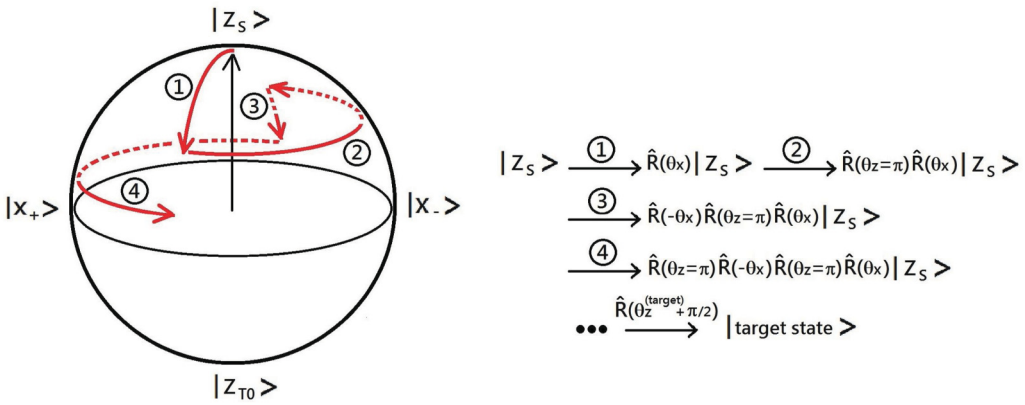

FIG. 2. (Color online) Single qubit manipulation, with the initial qubit state, e.g., $|zs\rangle$. One may apply the alternating sequence $R_x(\theta_x) \rightarrow R_z(\theta_z = \pi) \rightarrow R_x(-\theta_x) \rightarrow R_z(\theta_z = \pi) \rightarrow \ldots R_z(\theta_z^{(\text{target})} + \pi/2)$ and manipulate the initial state into a target state ($\theta_z^{(\text{target})}$ = target state longitude).

equation,

$$
\begin{aligned}
(H_D^{(0)} + H_A)\phi_D &= i\hbar\partial_t\phi_D, \\
H_D^{(0)} &= \begin{pmatrix} \Delta + V_{\text{QD}} & v_F\hat{p}_- \\ v_F\hat{p}_+ & -\Delta + V_{\text{QD}} \end{pmatrix}, \\
H_A &= \begin{pmatrix} 0 & ev_F A_- \\ ev_F A_+ & 0 \end{pmatrix}, \quad \phi_D = \begin{pmatrix} \varphi_A \\ \varphi_B \end{pmatrix}, \\
\hat{p}_- &= p_x - i\tau_v p_y, \hat{p}_+ = p_x + i\tau_v p_y, \\
A_- &= A_x - i\tau_v A_y, A_+ = A_x + i\tau_v A_y. \qquad (16)
\end{aligned}
$$

Here, $\boldsymbol{A} = (A_x, A_y)$ is the vector potential of the radiation field. $H_D^{(0)}$ is the QD Hamiltonian in the absence of radiation, and H_A is the light-electron interaction. We describe briefly the eigenstates of $H_D^{(0)}$ below. We denote $\phi_D^{(0,c)} = (\varphi_A^{(0,c)}, \varphi_B^{(0,c)})^{\text{T}}$ and $\phi_D^{(0,v)} = (\varphi_A^{(0,v)}, \varphi_B^{(0,v)})^{\text{T}}$ (T = transpose) as the lowest quantized conduction band state in the QD and the near-band-edge valence band state around the QD, respectively, with $E_0^{(c)}$ and $E_0^{(v)}$ being the corresponding energies. From Eq. (16),

$$
\begin{aligned}
\left(\varphi_A^{(0,c)}, \varphi_B^{(0,c)}\right)\big|_{\tau v=-1} &= \left(\varphi_A^{(0,c)*}, -\varphi_B^{(0,c)*}\right)\big|_{\tau v=1}, \\
\left(\varphi_A^{(0,v)}, \varphi_B^{(0,v)}\right)\big|_{\tau v=-1} &= \left(\varphi_A^{(0,v)*}, -\varphi_B^{(0,v)*}\right)\big|_{\tau v=1},
\end{aligned} \qquad (17)
$$

due to the time reversal symmetry between valley states in the absence of radiation. Moreover, for electrons near the gap, $|\varphi_A^{(0,c)}| \gg |\varphi_B^{(0,c)}|$ and $|\varphi_A^{(0,v)}| \ll |\varphi_B^{(0,v)}|$ for both $\tau_v = \pm 1$. In fact, it can be verified that

$$
\left|\varphi_B^{(0,c)}\right| / \left|\varphi_A^{(0,c)}\right| \sim \left|\varphi_A^{(0,v)}\right| / \left|\varphi_B^{(0,v)}\right| \sim O(E/\Delta)^{1/2}. \qquad (18)
$$

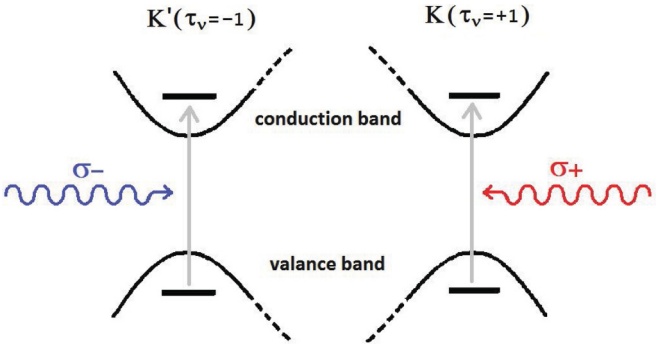

FIG. 3. (Color online) Approximate selection rule of optical excitation in gapped graphene.

We consider the near-resonance optical response of the QD to a normally incident light, in the form of a circularly polarized ($\sigma+$ or $\sigma-$) plane wave. The light-electron interaction in the case is given in the following:

$$
\begin{aligned}
&H_A|_{(\tau_v=1,\sigma+)\text{or}(\tau_v=-1,\sigma-)} \\
&= ev_F A_0 \left[e^{-i(k_{\text{ph}}z - w_{\text{ph}}t)} \begin{pmatrix} 0 & 1 \\ 0 & 0 \end{pmatrix} + e^{i(k_{\text{ph}}z - w_{\text{ph}}t)} \begin{pmatrix} 0 & 0 \\ 1 & 0 \end{pmatrix} \right], \\
&H_A|_{(\tau_v=-1,\sigma+)\text{or}(\tau_v=1,\sigma-)} \\
&= ev_F A_0 \left[e^{i(k_{\text{ph}}z - w_{\text{ph}}t)} \begin{pmatrix} 0 & 1 \\ 0 & 0 \end{pmatrix} + e^{-i(k_{\text{ph}}z - w_{\text{ph}}t)} \begin{pmatrix} 0 & 0 \\ 1 & 0 \end{pmatrix} \right],
\end{aligned}
$$

where k_{ph} is the photon wave vector, w_{ph} is the photon frequency, and A_0 is the amplitude of $\boldsymbol{A}$. H_A is treated with the time-dependent perturbation theory. We take $z = 0$ in the graphene plane. Then, near resonance ($w_{\text{ph}} \sim E_0^{(c)} - E_0^{(v)}$), the optical response is governed by the following optical matrix elements:

$$
\begin{aligned}
M_> &= ev_F A_0 \langle \varphi_A^{(c)} | \varphi_B^{(v)} \rangle, \text{ for } (\tau_\text{v} = 1, \sigma_+) \text{ or } (\tau_\text{v} = -1, \sigma_-), \\
M_< &= ev_F A_0 \langle \varphi_B^{(c)} | \varphi_A^{(v)} \rangle, \text{ for } (\tau_\text{v} = 1, \sigma_-) \text{ or } (\tau_\text{v} = -1, \sigma_+).
\end{aligned} \qquad (19)
$$

From the properties of wave functions listed in Eqs. (17) and (18), we obtain

$$
\begin{aligned}
M_>(\tau_y = 1) &= -M_>(\tau_y = -1)^*, \\
M_<(\tau_y = 1) &= -M_<(\tau_y = -1)^*, \qquad (20)
\end{aligned}
$$

$$
|M_<| / |M_>| \sim O(E/\Delta). \qquad (21)
$$

Equation (21) permits us to make the approximation that $M_<(\tau_v = \pm 1) = 0$, leading to the approximate selection rule that $|\text{K(valence)}\rangle + |\sigma+\rangle \rightarrow |\text{K(conduction)}\rangle$ and $|\text{K}'\text{(valence)}\rangle + |\sigma-\rangle \rightarrow |\text{K}'\text{(conduction)}\rangle$, mentioned previously in Sec. I and plotted in Fig. 3. Moreover, although derived for the band-to-band transition, the above result [see Eqs. (19)–(21)] applies to excitonic excitations as well, except

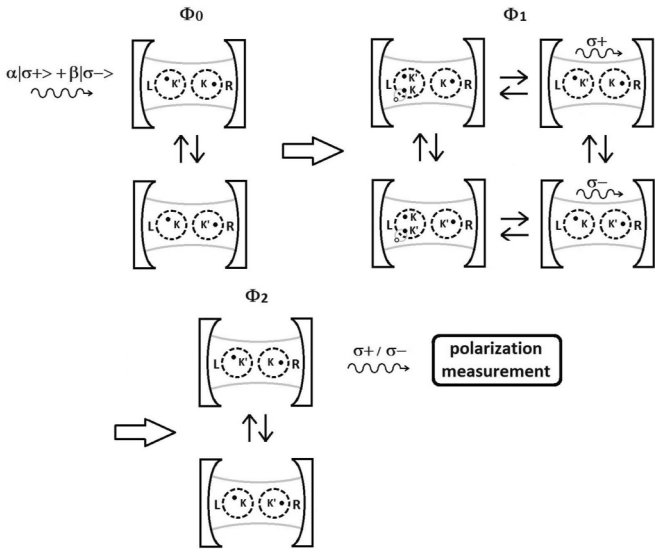

FIG. 4. The quantum state transfer from a photon qubit to a valley pair qubit. Dashed circles are quantum dots, black dots are the electrons, and white dots are the holes. Double arrows indicate resonance between states. For simplicity, in the state Φ_2 plotted here, we show the approximate polarization only, for the photon emitted by the exciton, as determined by the approximate selection rule in Eq. (1).

for an additional enhancement factor in the matrix element in Eq. (19), due to the sizable overlap of electron and hole wave functions in the exciton state.[26] Below, we denote $M_>(\tau_v = 1)$ simply as $M_>$, and $M_<(\tau_v = 1)$ as $M_<$.

Next, we describe a feasible method to transfer the quantum state from a photon qubit to a valley pair qubit, shown in Fig. 4, based on the optical response described in Eqs. (19)–(21) for the QD. To begin, the valley pair qubit is placed in a photonic cavity, and initialized in the singlet state $|\mathrm{K_L\,K'_R}\rangle - |\mathrm{K'_L\,K_R}\rangle$, with the exchange coupling J turned down after the initialization, in order to freeze the inter-QD orbital motion during the QST that follows. We take that the energy levels in $\mathrm{QD_L}$ and $\mathrm{QD_R}$ are detuned (by back gate voltages), and the cavity photon energy ($\hbar w_{\mathrm{cavity}}$) matches only the exciton binding energy ($\hbar w_{\mathrm{exciton}}$) in $\mathrm{QD_L}$. As shown in Fig. 4, the photon signal (with the photon frequency $w_{\mathrm{ph}} = w_{\mathrm{cavity}}$) enters the cavity in the polarization state $\alpha|\sigma+\rangle + \beta|\sigma-\rangle$ carrying the quantum information, and interact with the electrons in the QDs. Then, due to the light-electron interaction, the initial (photon-electron composite) state evolves in time. According to Eqs. (19)–(21), the following cavity QED processes take place in $\mathrm{QD_L}$, photon absorption:

$$
\begin{aligned}
|\Phi_0\rangle &= (|\mathrm{K_L K'_R}\rangle - |\mathrm{K'_L K_R}\rangle) \times (\alpha|\sigma+\rangle + \beta|\sigma-\rangle)\\
|\Phi_1\rangle &= (-\beta \mathrm{M}^*_> + \alpha \mathrm{M}_<)|\mathrm{K'_{exL} K_L K'_R}\rangle\\
&\quad - (\alpha \mathrm{M}_> - \beta \mathrm{M}^*_<)|\mathrm{K_{exL} K'_L K_R}\rangle,
\end{aligned}
$$

photon reemission ($\rightarrow$) and reabsorption ($\leftarrow$):

$$
\begin{aligned}
&|\Phi_1\rangle \leftrightarrow |\Phi_2\rangle\\
&\quad = (-\beta \mathrm{M}^*_> + \alpha \mathrm{M}_<)[-\mathrm{M}_>|\sigma - \mathrm{K_L K'_R}\rangle + \mathrm{M}^*_<)\\
&\qquad \times |\sigma + \mathrm{K_L K'_R}\rangle] - (\alpha \mathrm{M}_> - \beta \mathrm{M}^*_<)\\
&\qquad \times [\mathrm{M}^*_>|\sigma + \mathrm{K'_L K_R}\rangle - \mathrm{M}_<|\sigma - \mathrm{K'_L K_R}\rangle],
\end{aligned}
$$

where $|\Phi_0\rangle$ is the initial state, $\mathrm{K_{ex,L}}$ ($\mathrm{K'_{ex,L}}$) is the K (K′)-valley exciton created by the process of photon absorption in $\mathrm{QD_L}$. Note that the intermediate state $|\Phi_2\rangle$ generated in the above processes is entangled and the photon state can no longer be factored out in $|\Phi_2\rangle$. In this entangled state, the information carried by the photon is shared between photons and valley electrons. Eventually, the reemitted photon in $|\Phi_2\rangle$ escapes the cavity, and can be measured for its state of linear polarization, leaving the valley pair qubit carrying the full information. The measurement produces the valley pair state

$$
\begin{aligned}
|\Phi_{3\mathrm{x}}\rangle &= \langle \sigma_x|\phi_2\rangle\\
&= (-\beta \mathrm{M}^*_> + \alpha \mathrm{M}_<)(-\mathrm{M}_> + \mathrm{M}^*_<)|\mathrm{K_L K'_R}\rangle\\
&\quad - (\alpha \mathrm{M}_> - \beta \mathrm{M}^*_<)(\mathrm{M}^*_> - \mathrm{M}_<)|\mathrm{K'_L K_R}\rangle, \qquad (22)
\end{aligned}
$$

if x polarization is measured, or the state

$$
\begin{aligned}
|\Phi_{3\mathrm{y}}\rangle &= \langle \sigma_y \Phi_2\rangle\\
&= (-\beta \mathrm{M}^*_> + \alpha \mathrm{M}_<)(\mathrm{M}_> + \mathrm{M}^*_<)|\mathrm{K_L K'_R}\rangle\\
&\quad - (\alpha \mathrm{M}_> - \beta \mathrm{M}^*_<)(\mathrm{M}^*_> - \mathrm{M}_<)|\mathrm{K'_L K_R}\rangle, \qquad (23)
\end{aligned}
$$

if it yields y polarization.

In order to see that the above procedure indeed produces the desired photon $\rightarrow$ valley QST, we make the approximation $M_< = 0$ in Eqs. (22) and (23). Then, we see that

$$
|\Phi_{3x}\rangle \approx \beta|\mathrm{K_L K'_R}\rangle - \alpha|\mathrm{K'_L K_R}\rangle, \qquad (24)
$$

$$
|\Phi_{3y}\rangle \approx \beta|\mathrm{K_L K'_R}\rangle + \alpha|\mathrm{K'_L K_R}\rangle. \qquad (25)
$$

Thus the quantum information is successfully transferred to the valley pair qubit. If desired, one can further manipulate the qubit state in Eqs. (24) or (25) into the state $\alpha|\mathrm{K_L\,K'_R}\rangle + \beta|\mathrm{K'_L\,K_R}\rangle$ or $\alpha|z_S\rangle + \beta|z_{TO}\rangle$, with the VOI-based method described in Sec. III.

It is noted, in the QST mechanism envisioned above, that some information distortion [of $O(E/\Delta)$] appears to occur in the QST, as reflected in the contrast between Eqs. (22) and (23) and Eqs. (24) and (25), due to the finite magnitude of $M_<$. However, the distortion would only turn into a true loss of fidelity, if the transfer stands alone not being a part of a series of QSTs. As shall be shown below, in the back-to-back valley $\rightarrow$ photon $\rightarrow$ valley QST, the distortion of information in one transfer is cancelled by that in the other.

Let us now consider the valley $\rightarrow$ photon QST. We start with the following valley pair state in the cavity, $\alpha|\mathrm{K_L\,K'_R}\rangle + \beta|\mathrm{K'_L\,K_R}\rangle$, carrying quantum information. We send a photon into the cavity, with the photon initialized in the state $|\sigma+\rangle + |\sigma-\rangle$, and let it interact with the electrons. The photon-electron state evolves as follows: photon absorption,

$$
\begin{aligned}
|\Phi'_0\rangle &= (\alpha|\mathrm{K_L K'_R}\sim \mathrm{n} + \beta|\mathrm{K'_L K_R}\rangle) \times (|\sigma+\rangle + |\sigma-\rangle) \rightarrow\\
|\Phi'_1\rangle &= \alpha(M_< - M^*_>)|\mathrm{K'_{ex,L} K_L K'_R}\rangle\\
&\quad + \beta(M_> - M^*_<)|\mathrm{K_{ex,L} K'_L K_R}\rangle,
\end{aligned}
$$

and photon reemission ($\rightarrow$) and reabsorption ($\leftarrow$),

$$
\begin{aligned}
&|\Phi'_1\rangle \leftrightarrow |\Phi'_2\rangle\\
&\quad = \alpha(M_< - M^*_>)(-M_>|\sigma - \mathrm{K_L K'_R}\rangle + M^*_<|\sigma + \mathrm{K_L K'_R}\rangle)\\
&\qquad + \beta(M_> - M^*_<)(M^*_>|\sigma + \mathrm{K'_L K_R}\rangle - M_<|\sigma - \mathrm{K'_L K_R}\rangle).
\end{aligned}
$$

In $|\Phi_2'\rangle$, the reemitted photon and the QD electrons are entangled. The reemitted photon eventually escapes from the cavity, leaving behind the valley pair. We measure the valley pair state, producing the following photon state:

$$\begin{aligned}|\phi_{3S}'\rangle &= \langle z_S|\Phi_2'\rangle \\ &= [\alpha M_<^*(M_< - M_>^*) - \beta M_>^*(M_> - M_<^*)]|\sigma+\rangle \\ &\quad + [-\alpha M_>(M_< - M_>^*) + \beta M_<(M_> - M_<^*)]|\sigma-\rangle,\end{aligned} \tag{26}$$

if the measurement yields the singlet state, or

$$\begin{aligned}|\phi_{3T_0}'\rangle &= \langle z_{T_0}|\Phi_2'\rangle \\ &= [\alpha M_<^*(M_< - M_>^*) + \beta M_>^*(M_> - M_<^*)]|\sigma+\rangle \\ &\quad + [-\alpha M_>(M_< - M_>^*) + \beta M_<(M_> - M_<^*)]|\sigma-\rangle,\end{aligned} \tag{27}$$

if the triplet state is measured.

We remark on two points. Firstly, if we set $M_< = 0$ in Eqs. (26) and (27), we obtain

$$|\Phi_{3S}'\rangle = -\beta|\sigma+\rangle + \alpha|\sigma-\rangle, \tag{28}$$

$$|\Phi_{3T_0}'\rangle = \beta|\sigma+\rangle + \alpha|\sigma-\rangle, \tag{29}$$

showing a successful valley $\rightarrow$ photon QST. Again, because of the finite magnitude of $M_<$, the quantum information appears to be distorted in the QST, and would cause true fidelity loss of $O(E/\Delta)$, if the transfer is not coupled with other QSTs. Secondly, if we combine the results of Eqs. (22), (23), (26), and (27), it can be shown that the back-to-back QST is highly faithful, as expressed in the following diagram:

$$\begin{aligned}&\alpha|\mathrm{K_L K'_R}\rangle + \beta|\mathrm{K'_L K_R}\rangle \\ &\rightarrow^{\text{valley to photon}} \alpha'|\sigma+\rangle + \beta'|\sigma-\rangle \\ &\rightarrow^{\text{photon manipulation}} -\alpha'|\sigma+\rangle + \beta'|\sigma-\rangle \\ &\rightarrow^{\text{photon to valley}} \alpha|\mathrm{K_L K'_R}\rangle + \beta|\mathrm{K'_L K_R}\rangle.\end{aligned} \tag{30}$$

Here, $\alpha' = \alpha M_<^* e^{i\chi} - \beta M_>^*, \beta' = -\alpha M_> e^{i\chi} + \beta M_<$, and $e^{i\chi} = (M_< - M_>^*)/(M_> - M_<^*)$. In the diagram, we have assumed that the singlet state is measured in the valley $\rightarrow$ photon QST and that the x polarization is measured in the photon $\rightarrow$ valley QST. Faithful QST can also be shown with different results of measurement.

It is worth noting that, given the highly faithful back-to-back process shown above, a similar but longer process such as valley $\rightarrow$ photon $\rightarrow \ldots \rightarrow$ valley, which involves valley $\leftrightarrow$ photon QST for many times, is obviously, in principle, as faithful as the back-to-back process. That is, the small quantum distortion occurring in the single step valley $\leftrightarrow$ photon QST does not accumulate along the way. This is an important feature of the present valley-based approach for quantum memories, and is also an essential requirement for any quantum memories employed in long distance QCs. In reality, there are various factors which affect the yield and fidelity in the QST envisioned here, such as cavity Q factor and valley state decoherence. These important issues shall be studied in a separate work.

V. Summary and conclusion

In summary, we have investigated valley pair qubits in graphene double quantum dots, in the in-plane magnetic field configuration, and developed a method of qubit manipulation for this configuration. The method is based on the second-order relativistic-type effect in gapped graphene involving the valley-orbit interaction, and is able to operate in the time scale of $O(10$ ns). Moreover, the work has also considered the optical response of graphene quantum dots, in terms of valley excitation with respect to photonic polarization, and illustrated faithful quantum state transfers from photon to valley pair qubits and vice versa. It shows the potential of graphene quantum dots in photonic quantum communications, and in particular, the feasibility of implementing graphene-based quantum memories for quantum repeaters. Along with the previous exploration in Ref. 5 of valley pair qubits for quantum computing, it suggests the interesting prospect of an all-graphene approach for the solid state components of a quantum network, i.e., quantum computers and quantum memories in communications.

ACKNOWLEDGMENT

We thank the support of ROC National Science Council through the contract No. NSC100-2112-M-007-009.

APPENDIX A: THE SCHRODINGER-TYPE EQUATION IN GAPPED GRAPHENE, INCLUDING THE SECOND-ORDER RC

We derive the Schrodinger-type equation including the second-order RC, for near-band-edge electrons/holes in gapped graphene. Below, we consider only the case of electrons. (The case of holes can be worked out analogously.) We begin with the Dirac-type equation in the two-band model,

$$\begin{pmatrix} V-E & v_F\hat{p}_- \\ v_F\hat{p}_+ & -2\Delta + V - E \end{pmatrix}\begin{pmatrix}\varphi_A \\ \varphi_B\end{pmatrix} = 0.$$

Here, V is potential energy, E is the electron energy with respect to the conduction band edge, and $p_\pm = p_x \pm ip_y$. Or, equivalently,

$$\varphi_B = \frac{1}{2\Delta + E - V} v_F\hat{p}_+\varphi_A. \tag{A1}$$

$$H'\varphi_A = E\varphi_A, \quad H' = v_F\hat{p}_-\left(\frac{1}{2\Delta + E - V}v_F\hat{p}_+\right) + V, \tag{A2}$$

Equation (A1) is the first-order differential equation corresponding to the second row of the Dirac equation. Equation (A2) is a second-order differential equation obtained by combining the two first-order differential equations in the Dirac equation and is the primitive form of the Schrodinger equation to be derived.

We expand the energy denominator in Eq. (A2), up to the order $O(E^2/\Delta^2)$, giving

$$\begin{aligned}H' &\approx v_F\hat{p}_-\left\{\frac{1}{2\Delta}\left[1 - \frac{E-V}{2\Delta} + \left(\frac{E-V}{2\Delta}\right)^2\right]v_F\hat{p}_+\right\} + V \\ &= H^{(0)} + H'^{(1)} + H'^{(2)}.\end{aligned} \tag{A3}$$

Here,

$$H^{(0)} = p^2/2m^* + V \ (m^* = \Delta/v_F^2) \tag{A4}$$

deriving from the first term in [...] (and V), and constituting the "nonrelativistic" part of the "Schrodinger Hamiltonian." $H^{(1)}$' derives from the second term in [...] and constitutes the first-order RC. It was already given previously[5] and listed below:

$$H'^{(1)} = -\frac{1}{4m^*\Delta}\underline{\vec{p}V}\cdot\vec{p} - \frac{1}{4m^*\Delta}\underline{\vec{p}^2V} + \tau_v\frac{\hbar}{4m^*\Delta}\underline{\nabla V}\times\vec{p}. \tag{A5}$$

Here, terms underlined are evaluated first. We focus on the derivation of $H^{(2)}$ (the second-order RC) below.

There are two contributions to $H^{(2)}$', with one coming from the second term in [...] in (A3), and the other from the third term in [...]. We denote them as $H_2^{(2)}$ and $H^(2)_3$, respectively. We have

$$H'^{(2)} = H_2'^{(2)} + H_3'^{(2)}, \tag{A6}$$

$$\begin{aligned} H_2'^{(2)}\varphi_A &= -\frac{1}{2m^*}\hat{p}_-\left(\frac{E-V}{2\Delta}\right)\hat{p}_+\,\varphi_A|_{\text{second order}} \\ &= \frac{1}{32m^{*3}\Delta^2}\vec{p}^6\varphi_A + \frac{1}{16m^{*2}\Delta^2}\vec{p}^2\underline{\vec{p}^2V}\varphi_A \\ &\quad + \frac{1}{16m^{*2}\Delta^2}\vec{p}^2\underline{\vec{p}V}\cdot\vec{p}\varphi_A \text{ and} \\ &\quad - \tau_v\frac{\hbar}{16m^{*2}\Delta^2}\vec{p}^2\underline{\nabla V\times\vec{p}}\varphi_A, \end{aligned} \tag{A7}$$

$$\begin{aligned} H_3'^{(2)}\varphi_A &= \frac{1}{8m^*\Delta^2}\hat{p}_-[(E-V)^2\hat{p}_+\varphi_A] = R_1^{(2)} + R_2^{(2)}, \\ R_1^{(2)} &= \frac{1}{16m^{*2}\Delta^2}\left(\frac{1}{2m^*}\vec{p}^4\varphi_A + 2\underline{\vec{p}V}\cdot\underline{\vec{p}\varphi_A} + \underline{\vec{p}^2V}\varphi_A\right), \\ R_2^{(2)} &= \frac{1}{8m^{*2}\Delta^2}(\underline{\vec{p}V}\cdot\underline{\vec{p}\vec{p}^2\varphi_A} + \underline{\vec{p}^2V} \\ &\quad \cdot\underline{\vec{p}^2\varphi_A} - \tau_v\hbar\underline{\nabla V}\times\underline{\vec{p}\vec{p}^2\varphi_A}). \end{aligned} \tag{A8}$$

The ith results of Eqs. (A4), (A5), (A7), and (A8), it would appear that we have finished the derivation of the Schrodinger equation. However, it can be verified that several terms of H' as given in Eqs. (A5), (A7), and (A8) are not Hermitian and, hence, H' is not Hermitian. This is tied to the fact that the wave function φ_A used with the above Schodinger equation is not normalized, being just one of the two components in the Dirac wave function. This can be rectified by a similarity transformation as follows. We introduce the following transformation:

$$\begin{aligned} \varphi_A \to \psi = \Omega\varphi_A, \quad H' \to H = \Omega H'\Omega^{-1}, \\ \Omega = 1 + \Omega^{(1)} + \Omega^{(2)}, \quad \Omega^{(1)} = \frac{1}{8m^*\Delta}\vec{p}^2, \\ \Omega^{(2)} = \frac{-9}{128m^{*2}\Delta^2}\vec{p}^4 + \tau_v\frac{\hbar}{8m^*\Delta^2}\underline{\nabla V} \\ \times\vec{p} - \frac{1}{16m^*\Delta^2}\underline{\vec{p}^2\mathrm{V}}. \end{aligned}$$

It can be shown that the transformed wave function ψ is normalized to the second-order RC. With the above transformation, we obtain the Schrodinger equation:

$$\begin{aligned} H\psi &= E\psi, \quad H = H^{(0)} + H^{(1)} + H^{(2)}, \\ H^{(1)} &= -\frac{\vec{p}^4}{8m^{*2}\Delta} - \frac{1}{8m^*\Delta}\underline{\vec{p}^2V} + \tau_v\frac{\hbar}{4m^*\Delta}\underline{\nabla V}\times\vec{p}, \\ H^{(2)} &= \frac{\vec{p}^6}{16m^{*3}\Delta} - \frac{1}{64m^{*2}\Delta^2}\vec{p}^2V\vec{p}^2 + \frac{3}{64m^{*2}\Delta^2}\{\underline{\vec{p}^2V},\vec{p}^2\}_+ \\ &\quad + \frac{1}{128m^{*2}\Delta^2}\{\vec{p}^4,V\}_+ - \tau_v\frac{3\hbar}{32m^{*2}\Delta^2}\{\underline{\nabla V}\times\vec{p},\vec{p}^2\}_+. \end{aligned} \tag{A9}$$

In Eq. (A9), it is easy to verify that $H^{(0)}$ and $H^{(1)}$ are both Hermitian. Moreover, each $\{...\}_+$ in $H^{(2)}$ is the symmetrized product of two Hermitian operators and, consequently, $H^{(2)}$ is Hermitian. Altogether, it gives a Hermitian Hamiltonian H.

APPENDIX B: GEOMETRIC PHASE RATE OF CHANGE (γ_0) DUE TO THE ALTERNATING CURRENT ELECTRIC FIELD-INDUCED VOI-BASED EFFECT

We provide the perturbative evaluation of γ_0 due to the ac electric field-induced VOI-based effect. According to Sec. III, the rate of change in the geometric phase [see Eq. (7)] is

$$\gamma_0(t) = -(\partial_t y_0(t))\,\langle\varphi_0(x,y)|p_y\varphi_0(x,y)\rangle,$$

with $y_0(t) = 0$ in $\langle\varphi_0|p_y\varphi_0\rangle$. Here, $y_0(t) = \frac{e\varepsilon_y\sin w_s t}{m^* w_0^2}$ is the ac field-induced displacement, and φ_0 is determined by the following *time-independent* Schrodinger-type equation including up to the second-order RC, derived in Appendix A and presented in Sec. III:

$$\begin{aligned} H|_{y_0=0}\,\varphi_0(x,y) &= E_0\varphi_0(x,y), \quad H = H^{(0)} + V_3(x) + H', \\ H' &= H^{(1)} + H^{(2)}, \quad V_3(x) = \frac{1}{3}k_{3x}m^*w_0^2x^3, \end{aligned} \tag{B1}$$

$$\begin{aligned} H^{(0)}(x,y,t) &= \frac{\vec{p}^2}{2m^*} + V_2(x,y), \\ V_2(x,y) &= \frac{1}{2}m^*w_0^2(x^2+s^2y^2), \end{aligned} \tag{B2}$$

$$\begin{aligned} H^{(1)} &= H_0^{(1)} + H_\tau^{(1)}, \\ H_\tau^{(1)} &= \tau_v\frac{\hbar}{4m^*\Delta}[\nabla(V_2+V_3)]\times\vec{p} \ \text{(first}-\text{order VOI)}, \\ H_0^{(1)} &= -\frac{\vec{p}^4}{8m^{*2}\Delta} - \frac{1}{8m^*\Delta}(\vec{p}^2V_2) - \frac{1}{8m^*\Delta}(\vec{p}^2V_3) \\ &\quad \to H_{02}^{(1)} + H_{03}^{(1)} \\ H_{02}^{(1)} &= -\frac{p^4}{8m^{*2}\Delta}, \quad H_{03}^{(1)} = -\frac{1}{8m^*\Delta}(\vec{p}^2V_3), \end{aligned} \tag{B3}$$

$$\begin{aligned} H^{(2)} &= H_0^{(2)} + H_\tau^{(2)}, \\ H_\tau^{(2)} &= H_{\tau 2}^{(2)} + H_{\tau 3}^{(2)} \ \text{(second}-\text{order VOI)}, \\ H_{\tau 2}^{(2)} &= -\tau_v\frac{3\hbar}{32m^{*2}\Delta^2}[\underline{\nabla V_2\times\vec{p}}\vec{p}^2 + \vec{p}^2\underline{\nabla V_2\times\vec{p}}], \\ H_{\tau 3}^{(2)} &= -\tau_v\frac{3\hbar}{32m^{*2}\Delta^2}[\underline{\nabla V_3\times\vec{p}}\vec{p}^2 + \vec{p}^2\underline{\nabla V_3\times\vec{p}}]. \end{aligned} \tag{B4}$$

Note that in Eq. (3) the term $\frac{1}{8m^*\Delta}(\vec{p}^2V_2)$ in $H_0^{(1)}$ has been dropped, being only a constant. According to Sec. III, we

write

$$\langle\varphi_0(x,y)|p_y\varphi_0(x,y)\rangle \approx p_y^{(1)} + p_y^{(2,1)} + p_y^{(2,2)} \propto \tau_v k_{3x}, \tag{B5}$$

which is correct to the second-order RC, where $p_y^{(1)}$ is the first-order RC and derives from $H_\tau^{(1)}$ in the first-order perturbative treatment of H'. $p_y^{(2,1)}$ denotes the second-order RC, deriving from $H_\tau^{(1)}$, in the second-order perturbative treatment of H'. $p_y^{(2,2)}$ denotes the second-order RC, deriving from $H_\tau^{(2)}$, in the first-order perturbative treatment of H'. We calculate the three foregoing momentum matrix elements below.

Firstly, we show that $p_y^{(1)} = 0$. Because $p_y^{(1)}$ is first order in RC, it simplifies by writing

$$p_y^{(1)} = \langle\varphi_0'|p_y\varphi_0'\rangle, (H^{(0)} + V_3 + H_0^{(1)} + H_\tau^{(1)})\varphi_0' = E_0'\varphi_0',$$

where φ_0 in $p_y^{(1)}$ has been replaced by φ_0', the ground-state solution correct only to the first-order RC. Note that it suffices to evaluate φ_0' here with the first-order perturbation theory treating $H_0^{(1)}$ and $H_\tau^{(1)}$ as the perturbation.

Since $p_y^{(1)} \propto \tau_v$, only the perturbative correction due to $H_\tau^{(1)}$ contributes to $p_y^{(1)}$. We thus drop $H_0{}^{(1)}$ in the Schrodinger equation and rewrite

$$p_y^{(1)} = \langle\varphi_0'|p_y\varphi_0'\rangle, (H^{(0)} + V_3 + H_\tau^{(1)})\varphi_0' = E_0'\varphi_0'.$$

(The same notation φ_0' shall be used repeatedly where it causes no confusion.) Applying Ehrenfest's theorem to the following expectation value involving the last φ_0',

$$0 = \frac{\mathrm{d}\langle\varphi_0'|\mathrm{y}|\varphi_0'\rangle}{\mathrm{dt}} = -\frac{i}{\hbar}\langle\varphi_0'|\left(y, H^{(0)} + V_3 + H_\tau^{(1)}\right)|\varphi_0'\rangle,$$

we obtain

$$p_y^{(1)} = -\tau_v\frac{\hbar}{4\Delta}\langle\varphi_0'|\partial_x V_{23}|\varphi_0'\rangle,$$

where $V_{23} = V_2 + V_3$. The above procedure has extracted out an order of RC and provided a new expression of expectation value ($\langle\varphi_0'|\partial_x V_{23}|\varphi_0'\rangle$ here), which can be evaluated at a lower order of RC. With this, we can further simplify $p_y^{(1)}$, while still keeping it correct to the first-order RC, by writing

$$p_y^{(1)} = -\tau_v\frac{\hbar}{4\Delta}\langle\varphi_0'|\partial_x V_{23}|\varphi_0'\rangle, (H^{(0)} + V_3)\varphi_0' = E_0'\varphi_0',$$

where the wave equation now includes no RC at all. Then, applying again Ehrenfest's theorem,

$$0 = \frac{\mathrm{d}\langle\varphi_0'|\mathrm{p_x}|\varphi_0'\rangle}{\mathrm{dt}} = -\frac{i}{\hbar}\langle\varphi_0'|[\mathrm{p_x}, H^{(0)} + V_3|\varphi_0'\rangle,$$

one obtains

$$p_y^{(1)} \propto \langle\varphi_0'|\partial_x V_{23}|\varphi_0'\rangle = 0.$$

With $p_y^{(1)} = 0$ as just shown, we rewrite Eq. (B5),

$$\langle\varphi_0(x,y)|p_y\varphi_0(x,y)\rangle \approx p_y^{(2,1)} + p_y^{(2,2)} \propto \tau_v k_{3x}\left(\frac{\hbar w_0}{\Delta}\right)^2, \tag{B6}$$

expressing explicitly that the momentum matrix element and, hence, γ_0 as well are finite only at the second-order RC.

Before we move on to calculate the momentum matrix elements remaining in Eq. (B6), we summarize the useful trick employed above in the derivation of $p_y^{(1)}$, since it is to be utilized again in the evaluation of these matrix elements. Namely, we utilize Ehrenfest's theorem to extract out τ_v, k_{3x}, and the order of RC as well, from the expectation value being evaluated, and then proceed with the perturbation theory at a lower order to calculate the new expectation value appearing after the extraction.

We calculate $p_y^{(2,1)}$ in Eq. (B6) now. Because $p_y^{(2,1)}$ derives from $H_\tau^{(1)}$, in the second-order perturbative treatment of H' (or, rather, the part of $H^{(1)}$ only), we write

$$p_y^{(2,1)} = \langle\varphi_0'|p_y|\varphi_0'\rangle, (H^{(0)} + V_3 + H^{(1)})\varphi_0' = E_0'\varphi_0'.$$

In addition, being linear in k_{3x}, $p_y^{(2,1)}$ is first order in V_3. Altogether, the calculation of $p_y^{(2,1)}$ would be a third-order perturbative treatment, if one calculates $p_y^{(2,1)}$ straightforwardly using the eigenstates of H_0 (which are harmonic oscillator wave functions) and treating both V_3 and $H^{(1)}$ as perturbations. We have evaluated $p_y^{(2,1)}$ in this lengthy way. On the other hand, an alternative calculation has been developed which agrees with the lengthy one but reduces the treatment to a second-order perturbative calculation, based on the trick summarized earlier. Below, we present the second method. We apply the trick and write

$$\begin{aligned}
&\langle\varphi_0'|p_y|\varphi_0'\rangle \ \left(\text{Ehrenfest's theorem} : 0 = \frac{\mathrm{d}\langle\varphi_0'|\mathrm{y}|\varphi_0'\rangle}{\mathrm{dt}}\right.\\
&= -\frac{m^*}{i\hbar}\langle\varphi_0'|[y, H^{(1)}]|\varphi_0'\rangle = \langle\varphi_0'|[\mathrm{y}, \mathrm{H}^{(0)} + V_3 + \mathrm{H}^{(1)}]|\varphi_0'\rangle.)\\
&= -m^*\langle\varphi_0'|\partial_{p_y}H^{(1)}|\varphi_0'\rangle = p_3^{(2,1)} + p_\tau^{(2,1)} + p_0^{(2,1)},\\
&p_3^{(2,1)} = -m^*\langle\varphi_0'|\partial_{p_y}H_{03}^{(1)}|\varphi_0'\rangle = 0,\\
&p_\tau^{(2,1)} = -m^*\langle\varphi_0'|\partial_{p_y}H_\tau^{(1)}|\varphi_0'\rangle = -\tau_v\frac{\hbar}{4\Delta}\langle\varphi_0'|\partial_x V_{23}|\varphi_0'\rangle,\\
&p_2^{(2,1)} = -m^*\langle\varphi_0'|\partial_{p_y}H_{02}^{(1)}|\varphi_0'\rangle.
\end{aligned} \tag{B7}$$

We focus now on the last two matrix elements introduced in Eq. (B7). Firstly, we reduce $p_\tau^{(2,1)}$ by writing

$$\begin{aligned}
p_\tau^{(2,1)} &= -\tau_v\frac{\hbar}{4\Delta}\langle\varphi_0'|\partial_x V_{23}|\varphi_0'\rangle,\\
&(H^{(0)} + V_3 + H_{02}^{(1)} + H_{03}^{(1)})\varphi_0' = E_0'\varphi'_0.
\end{aligned}$$

Utilizing Ehrenfest's theorem, we have

$$\begin{aligned}
p_\tau^{(2,1)} &= -\tau_v\frac{\hbar}{4\Delta}\langle\varphi_0'|\partial_x V_{23}|\varphi_0'\rangle\\
&= \tau_v\frac{\hbar}{4\Delta}\langle\varphi_0'|\partial_x H_{03}^{(1)}|\varphi_0'\rangle = -\tau_v\frac{\hbar}{16}\frac{\hbar^2 w_0^2}{\Delta^2}k_{3x}.
\end{aligned} \tag{B8}$$

We turn to the calculation of $p_2^{(2,1)}$ in Eq. (B7). We start by reducing $p_2^{(2,1)}$,

$$\begin{aligned}
p_2^{(2,1)} &= -m^*\langle\varphi_0'|\partial_{p_y}H_{02}^{(1)}|\varphi_0'\rangle,\\
(H^{(0)} + V_3 + H_\tau^{(1)})\varphi_0' &= E_0'\varphi_0'.
\end{aligned}$$

Note that φ_0' here needs to be evaluated only to the second order in the perturbation $V_3 + H_\tau^{(1)}$. This can be carried out,

yielding

$$p_2^{(2,1)} = -\tau_v \frac{s}{64}\left[-2 - \frac{16}{3(s+1)} + \frac{50}{3(s+2)}\right]\hbar\frac{\hbar^2 w_0^2}{\Delta^2}k_{3x}. \quad \text{(B9)}$$

Collecting the results in Eqs. (B7)–(B9), we obtain

$$p_y^{(2,1)} = -\tau_v \frac{s}{64}\left[-2 + \frac{4}{s} - \frac{16}{3(s+1)} + \frac{50}{3(s+2)}\right]\hbar\frac{\hbar^2 w_0^2}{\Delta^2}k_{3x}. \quad \text{(B10)}$$

Last, we evaluate $p_y{}^{(2,2)}$ in Eq. (B6). Because it derives from $H_\tau{}^{(2)}$ in the first-order perturbative treatment of H', we write

$$p_y^{(2,2)} = \langle\varphi_0'|p_y|\varphi_0'\rangle, (H^{(0)} + V_3 + H_\tau^{(2)})\varphi_0' = E_0'\varphi_0'.$$

Utilizing Ehrenfest's theorem, we write

$$\begin{aligned} p_y^{(2,2)} &= -m^*\langle\varphi_0'|\partial_{p_y}H_\tau^{(2)}|\varphi_0'\rangle = p_2^{(2,2)} + p_3^{(2,2)},\\ p_2^{(2,2)} &= -m^*\langle\varphi_{02}'|\partial_{p_y}H_{\tau 2}^{(2)}|\varphi_{02}''\rangle,\\ (H^{(0)} + V_3)\varphi_{02}' &= E_{02}'\varphi_{02}',\\ p_3^{(2,2)} &= -m^*\langle\varphi_{03}'|\partial_{p_y}H_{\tau 3}^{(2)}|\varphi_{03}'\rangle,\\ H^{(0)}\varphi_{03}' &= E_{03}'\varphi_{03}'. \end{aligned} \quad \text{(B11)}$$

Two matrix elements, $p_2{}^{(2,2)}$ and $p_3{}^{(2,2)}$, have been introduced here. $p_2{}^{(2,2)}$ can be calculated with φ_{02}' evaluated perturbatively to the first order of V_3, yielding

$$p_2^{(2,2)} = \tau_v\frac{(9s+1)}{64}\hbar\frac{\hbar^2 w_0^2}{\Delta^2}k_{3x}. \quad \text{(B12)}$$

As for $p_3{}^{(2,2)}$, with φ_{03}' being the ground-state harmonic oscillator wave function, it can be calculated straightforwardly, yielding

$$p_3^{(2,2)} = -\tau_v\frac{3(3s-1)}{64}\hbar\frac{\hbar^2 w_0^2}{\Delta^2}k_{3x}. \quad \text{(B13)}$$

Collecting the results in Eqs. (B11)–(B13), we obtain

$$p_y^{(2,2)} = \tau_v\frac{1}{16}\hbar\frac{\hbar^2 w_0^2}{\Delta^2}k_{3x}. \quad \text{(B14)}$$

In summary, we have derived and listed in Eqs. (B6), (B10), and (B14) all the momentum matrix elements appearing in Eq. (7) for the evaluation of the geometric phase rate of change (γ_0).

APPENDIX C: COHERENCE TIME OF VALLEY PAIR QUBIT IN THE IN-PLANE MAGNETIC FIELD CONFIGURATION

We estimate the coherence time of valley pair qubits. In the absence of a normal magnetic field, the valley states are degenerate, and the qubit decoherence derives primarily from the elastic intervalley scattering K $\leftrightarrow$ K′ in each QD. Accordingly, the coherence time is determined by the following valley flip rate:

$$\frac{\hbar}{\tau_{\mathrm{K}\leftrightarrow\mathrm{K}'}} \approx O(V_{\mathrm{K}\leftrightarrow\mathrm{K}'}). \quad \text{(C1)}$$

Here, $\tau_{K\leftrightarrow K'}$ is the valley flip time and

$$V_{\mathrm{K}\leftrightarrow\mathrm{K}'} = \text{intervalleycoupling} = \langle \mathrm{K_D}|V_{\mathrm{QD}}|\mathrm{K'}_{\mathrm{D}}\rangle, \quad \text{(C2)}$$

$\mathrm{K_D}$ and $\mathrm{K_D}$' being the quantized valley states in the QD. We write

$$|K_D\rangle = \phi_{\mathrm{K}}(\vec{r})e^{i\vec{K}\cdot\vec{r}}u_{\mathrm{K}}, \quad |K_D\rangle = \phi_{\mathrm{K}'}(\vec{r})e^{i\vec{K}'\cdot\vec{r}}u_{\mathrm{K}'}, \quad \text{(C3)}$$

where ϕ_{K} and $\phi_{\mathrm{K}'}$ are envelope functions, and u_{K} and $u_{\mathrm{K}'}$ are the Bloch cell-periodic functions at K and K′ points, respectively. Equations (C1) and (C2) show that $\tau_{\mathrm{K}\leftrightarrow\mathrm{K}'}$ depends on the profile of V_{QD}, which provides in the intervalley scattering the large wave vector difference (δk) between $|\mathrm{K_D}\rangle$ and $|\mathrm{K'_D}\rangle$ [with $\delta k \sim O(|\mathbf{K} - \mathbf{K}'|) \sim O(A^{-1})$].

In the following, we consider the regime where $\delta k\, L \gg 1$ (L = QD size) and estimate $V_{\mathrm{K}\leftrightarrow\mathrm{K}'}$ in Eq. (C2) with three profiles of V_{QD}. We take L (QD size) ~300 Å and potential depth $V_0 \sim 0.1$ eV, for typical applications of valley pair qubits.[5] We employ the following approximation:

$$\begin{aligned} V_{\mathrm{K}\leftrightarrow\mathrm{K}'} &= \langle \mathrm{K'}_D|V_{\mathrm{QD}}|\mathrm{K}_D\rangle \approx O\left(\frac{1}{L^2}\int_{r\leqslant L} V_{\mathrm{QD}}(\vec{r})e^{-i\delta k\cdot\vec{r}}d^2r\right),\\ \overrightarrow{\delta k} &= \vec{\mathbf{k}} - \vec{\mathbf{k}}', \end{aligned} \quad \text{(C4)}$$

where the envelope functions ϕ_{K} and $\phi_{\mathrm{K}'}$ in Eq. (C4) are taken approximately to be constant for $r < L$ and zero for $r > L$. Equation (C4) is basically the Fourier transform of V_{QD} at $\boldsymbol{\delta}\mathbf{k}$ and suffices for the order-of-magnitude estimate of $V_{\mathrm{K}\leftrightarrow\mathrm{K}'}$.

Firstly, we consider (a) an ideal square well, with barrier height V_0. This is the worst case scenario, since the abrupt change in the potential leads to sizable Fourier components at large wave vectors and causes frequent intervalley scattering, resulting in short $\tau_{\mathrm{K}\leftrightarrow\mathrm{K}'}$. A brief dimensional analysis with Eq. (C4) in the case shows that

$$V_{\mathrm{K}\leftrightarrow\mathrm{K}'} \approx O\left[\frac{V_0}{(L\delta k)^2}\right] \approx O(\mu\mathrm{eV}) \quad \text{or} \quad \tau_{\mathrm{K}\leftrightarrow\mathrm{K}'} \approx O(10\mathrm{ns}). \quad \text{(C5)}$$

The coherence time is close to the time needed for VOI-based manipulation of qubits [$\sim O(10$ ns)].

Next, we consider (b) a realistic square well, with a transition region between well and barrier. For the convenience of analysis, we simulate V_{QD} in this case with a factorizable form, such that the integral in (C-4) can be decomposed into the product of two independent one-dimensional integrals. We take $V_{\mathrm{QD}} = V_{1/2}(x)V_{1/2}(y), V_{1/2}(x) = (V_0)^{1/2}$ for $-L' < x < L'$; $V_{1/2}(x) = (V_0)^{1/2}(x+L)/(L-L')$ for $-L < x < -L'$; $V(x) = (V_0)^{1/2}(L-x)/(L-L')$, for $L' < x < L$; and $V(x) = 0$ elsewhere. $V_{1/2}(y) = -V_{1/2}(x)|_{x\to y}$. We also take $O(L') \sim O(L)$ and the transition layer thickness $\delta L(= L - L') \sim 0.1L$. With this factorizable potential, we obtain

$$V_{\mathrm{K}\leftrightarrow\mathrm{K}'} = -(\overline{V}_{1/2})^2, \quad \overline{V}_{1/2} = O\left[\frac{1}{L}\int_{-L}^{L} V_{1/2}(x)e^{-i\delta k\cdot x\hat{x}}dx\right].$$

Analysis of the one-dimensional integral appearing here gives

$$\overline{V}_{1/2} \approx O\left[\frac{V_0^{1/2}}{(L\delta k)(\delta L\delta k)}\right],$$
$$V_{\mathrm{K}\leftrightarrow\mathrm{K}'} \approx O\left[\frac{V_0}{(L\delta k)^2(\delta L\delta k)^2}\right] \approx O(1\mathrm{neV}),$$
$$\text{or} \quad \tau_{\mathrm{K}\leftrightarrow\mathrm{K}'} \approx O(0.5\mu\mathrm{s}). \tag{C6}$$

The valley flip time here is long enough for qubit manipulation.

Last, we consider (c) a parabolic potential, $V_{\mathrm{QD}} = {}^1\!/_2 m^* w_0^2 r^2$, with $\hbar w_0 \sim O(V_0)$. In this case, we obtain

$$V_{\mathrm{K}\leftrightarrow\mathrm{K}'} \approx O\left[\frac{V_0}{(L\delta k)^4}\right] \approx O(0.01\mathrm{neV}) \text{ or } \tau_{\mathrm{K}\leftrightarrow\mathrm{K}'} \approx O(50\mu\mathrm{s}). \tag{C7}$$

It provides a very long coherence time for the qubit manipulation. Comparing the results in Eqs. (C5)–(C7), we see that the qubit coherence time can be increased significantly with a QD profile engineering that is able to create a smooth QD confinement potential.

*E-mail: yswu@ee.nthu.edu.tw

[1] C. H. Bennett, G. Brassard, C. Crepeau, R. Jozsa, A. Peres, and W. Wootters, Phys. Rev. Lett. **70**, 1895 (1993).

[2] H. J. Briegel, W. Dur, J. I. Cirac, and P. Zoller, Phys. Rev. Lett. **81**, 5932 (1998); L.-M. Duan, M. D. Lukin, J. J. Cirac, and P. Zoller, Nature **414**, 413 (2001); E. Togan, Y. Chu, A. S. Trifonov, L. Jiang, J. Maze, L. Childress, M. V. G. Dutt, A. S. Sørensen, P. R. Hemmer, A. S. Zibrov, and M. D. Lukin, Nature (London) **466**, 7307 (2010).

[3] D. Deutsch, Proc. R. Soc. London A **400**, 97 (1985); P. W. Shor, in *Proceedings of the 35th Annual Symposium on Foundations of Computer Science*, edited by S. Goldwasser (IEEE Computer Society Press, Los Alamitos, CA, 1994); L. K. Grover, Phys. Rev. Lett. **79**, 325 (1997); M. A. Nielsen and I. L. Chuang, *Quantum Computation and Quantum Information* (Cambridge University Press, 2003).

[4] D. Loss and D. P. DiVincenzo, Phys. Rev. A **57**, 120 (1998); G. Burkard, D. Loss, and D. P. DiVincenzo, Phys. Rev. B **59**, 2070 (1999); B. Trauzettel, D. B. Bulaev, D. Loss, and G. Burkard, Nat. Phys. **3**, 192 (2007).

[5] G. Y. Wu, N.-Y. Lue, and L. Chang, arXiv:1104.0443; Phys. Rev. B **84**, 195463 (2011).

[6] K. S. Novoselov, A. K. Geim, S. V. Morozov, D. Jiang, Y. Zhang, S. V. Dubonos, I. V. Grigorieva, and A.A. Firsov, Science **306**, 666 (2004); A. K. Geim and K. S. Novoselov, Nat. Mater. **6**, 183 (2007).

[7] A. H. Castro Neto, F. Guinea, N. M. R. Peres, K. S. Novoselov, and A. K. Geim, Rev. Mod. Phys. **81**, 109 (2009).

[8] A. Rycerz, J. Tworzydlo, and C. W. J. Beenakker, Nat. Phys. **3**, 172 (2007).

[9] S. Y. Zhou, G.-H. Gweon, A. V. Fedorov, P. N. First, W. A. de Heer, D.-H. Lee, F. Guinea, A. H. Castro Neto, and A. Lanzara,, Nat. Mater. **6**, 770 (2007).

[10] G. Giovannetti, P. A. Khomyakov, G. Brocks, P. J. Kelly, and J. van den Brink, Phys. Rev. B **76**, 073103 (2007).

[11] D. Xiao, W. Yao, and Q. Niu, Phys. Rev. Lett. **99**, 236809 (2007).

[12] P. Recher, B. Trauzettel, A. Rycerz, Ya. M. Blanter, C. W. J. Beenakker, and A. F. Morpurgo, Phys. Rev. B **76**, 235404 (2007).

[13] E. I. Rashba and A. L. Efros, Phys. Rev. Lett. **91**, 126405 (2003).

[14] J. M. Taylor, H. M. Engel, W. Dur, A. Yacoby, C. M. Markus, P. Zoller, and D. Lukin, Nat. Phys. **1**, 177 (2005); S. Nadj-Perge, S. M. Frolov, E. P. A. M. Bakkers, and L. P. Kouwenhoven, Nature (London) **468**, 1084 (2010).

[15] C. H. Bennett, G. Brassard, and A. K. Ekert, Sci. Am. **267**, 50 (1992).

[16] N. Sangouard, C. Simon, H. de Riedmatten, and N. Gisin, Rev. Mod. Phys. **83**, 33 (2011).

[17] M. Żukowski, A. Zeilinger, M.A. Horne, and A.K. Ekert, Phys. Rev. Lett. **71**, 4287 (1993).

[18] R. Vrijen and E. Yablanovitch, Physica E **10**, 569 (2001); Y. Rikitake, H. Imamura, and H. Kosaka, J. Phys. Soc. Jpn. **76**, 114004 (2007).

[19] W. Yao, D. Xiao, and Q. Niu, Phys. Rev. B **77**, 235406 (2008).

[20] The impurity-caused intervalley scattering in a gapless graphene sheet is discussed by A. F. Morpurgo and F. Guinea, Phys. Rev. Lett. **97**, 196804 (2006).

[21] D. A. Lidar, I. L. Chuang, and K. B. Whaley, Phys. Rev. Lett. **81**, 2594 (1998); M. Mohseni and D. A. Lidar, *ibid.* **94**, 040507 (2005).

[22] J. Levy, Phys. Rev. Lett. **89**, 147902 (2002).

[23] D. P. DiVincenzo, Phys. Rev. A **51**, 1015 (1995); T. Sleator and H. Weinfurter, Phys. Rev. Lett. **74**, 4087 (1995); A. Barenco, Pro. R. Soc. Lond. A **449**, 679 (1995).

[24] The first-order RC in gapped graphene is discussed by P. Gosselin, A. Berard, H. Mohrbach, and S. Ghosh, Eur. Phys. J. C **59**, 883 (2009), and also by Wu *et al.*in Ref. 5.

[25] M. Born and V. A. Fock, Zeitschrift für Physik A **51**, 165 (1928).

[26] See, for example, O. Madelung, *Introduction to Solid-State Theory* (Springer, 1978).